ARTICLE IN PRESS

Available online at www.sciencedirect.com

SciVerse ScienceDirect

Proceedings of the Combustion Institute xxx (2012) xxx–xxx

Proceedings of the Combustion Institute

www.elsevier.com/locate/proci

Finding thermoacoustic limit cycles for a ducted Burke–Schumann flame

Simon J. Illingworth *, Iain C. Waugh, Matthew P. Juniper

University of Cambridge, Department of Engineering, Trumpington Street, Cambridge CB2 1PZ, UK

Abstract

This paper examines nonlinear thermoacoustic oscillations of a ducted Burke–Schumann diffusion flame. The nonlinear dynamics of the thermoacoustic system are studied using two distinct approaches. In the first approach, a continuation analysis is performed to find limit cycle amplitudes over a range of operating conditions. The strength of this approach is that one can characterize the coupled system's nonlinear behaviour over a large parameter space with relative ease. It is not able to give physical insight into that behaviour, however. The second approach uses a Flame Describing Function (FDF) to characterize the flame's response to harmonic velocity fluctuations over a range of forcing frequencies and forcing amplitudes, from which limit cycle amplitudes can be found. A strength of the FDF approach is that it reveals the physical mechanisms responsible for the behaviour observed. However, the calculation of the FDF is time consuming, and it must be recalculated if the flame's operating conditions change. With the strengths and shortcomings of the two approaches in mind, this paper advocates combining the two to provide the dynamics over a large parameter space and, furthermore, physical insight into that behaviour at judiciously-chosen points in the parameter space. Further physical insight concerning the flame's near-linear response at all forcing amplitudes is given by studying the forced flame in the time domain. It is shown that, for this flame model, the limit cycles arise because of the flame's nonlinear behaviour when it is close to the inlet.

Keywords: Thermoacoustics; Combustion oscillations; Diffusion flame; Flame describing function; Continuation analysis

1. Introduction

Thermoacoustic oscillations can occur whenever combustion takes place inside an acoustic resonator. Unsteady combustion is an efficient acoustic source [1], and combustors tend to be highly resonant systems. Therefore for suitable phase between unsteady combustion and acoustic perturbations, large-amplitude self-excited oscillations can occur.

Most recent studies of combustion oscillations have focused on low NO_x premixed gas turbine combustors, which are particularly susceptible to thermoacoustic instability [2,3]. These studies typically assume linear acoustics: the low Mach number means that the acoustic pressure fluctuations are small even when the acoustic velocity fluctuations are large [4]. The heat release is therefore treated as the nonlinear element in the coupled system.

* Corresponding author.
E-mail address: si250@cam.ac.uk (S.J. Illingworth).

1540-7489/$ - see front matter © 2012 Published by Elsevier Inc. on behalf of The Combustion Institute.
http://dx.doi.org/10.1016/j.proci.2012.06.017

Few studies have focused on non-premixed combustors [5–8], even though most gas turbines operate under non-premixed or partially-premixed conditions and are also susceptible to thermoacoustic oscillations (albeit less so). In this paper we therefore consider thermoacoustic oscillations in an acoustic resonator containing a Burke–Schumann flame, which is a simple model of a non-premixed flame. We consider linear acoustics and nonlinear heat release, and our main focus is the nonlinear behaviour of the coupled system.

Figure 1 shows the steady state amplitude, a_s, for two types of nonlinear behaviour that we expect to find. The first is a supercritical bifurcation, in which the limit cycle amplitude grows gradually as the control parameter, P, increases past P_l (P_l denotes the Hopf bifurcation, at which point the system becomes linearly unstable). The second is a subcritical bifurcation, in which the limit cycle amplitude grows suddenly as P increases past P_l, and for which there are two stable solutions in the region $P_c \leqslant P \leqslant P_l$.

Limit cycles can be found in the frequency domain using a Flame Describing Function (FDF), which involves measuring the flame's response to harmonic forcing for different forcing frequencies and forcing amplitudes. By assuming that the flame's response to a given forcing frequency is predominately at that frequency (i.e. by discarding higher harmonics), the FDF provides the flame's gain and phase as a function of forcing frequency and forcing amplitude. Dowling [9, Fig. 10] calculates the FDF for a kinematic model of a premixed ducted flame and finds that the limit cycle amplitude of her coupled system is determined by the amplitude-dependence of the gain. Noiray et al. [10] measure the FDF of a premixed flame experimentally and find that the limit cycle amplitude of their coupled system is determined by the amplitude-dependence of both the gain and the phase of the flame's response. At this point it is important to relate the describing function analysis (in particular, its description of the variations in the flame's gain and phase with forcing amplitude) to the supercritical and subcritical bifurcations seen in Fig. 1. If the flame's phase does not change with forcing amplitude, then one would expect to find only supercritical bifurcations (provided that the flame's gain decreases with increasing forcing amplitude, which is a sensible assumption). This is because as the forcing amplitude increases, the positive feedback between unsteady heat release and acoustics can only weaken, since the flame's gain is decreasing, while the phase between them remains fixed. If both the gain and the phase vary, however, then both supercritical and subcritical bifurcations are possible. In this case, even if we assume that the flame's gain decreases with increasing forcing amplitude as before, variations in phase can actually lead to stronger positive feedback between unsteady heat release and acoustics. Now relating these considerations to previous studies: the variations in the flame's phase with forcing amplitude seen by Dowling are either zero [4] or small [9], and so only supercritical behaviour is seen; while in Noiray et al. [10], the experimentally-determined FDF exhibits appreciable changes in both gain and phase, and so both types of bifurcation behaviour are seen (and predicted).

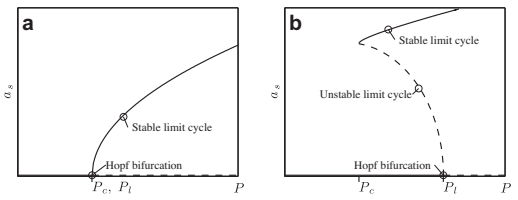

Fig. 1. The limit cycle amplitude, a_S, as a function of a control parameter, P, for (a) a supercritical bifurcation and (b) a subcritical bifurcation. P_l is the Hopf point, where the system becomes linearly unstable. P_c is the point below which no oscillations can be sustained.

Limit cycles can also be found in the time domain. This can be achieved using continuation analysis of the governing equations of the coupled system (to be described in Section 3). Continuation analysis finds a limit cycle and tracks its evolution as the system parameters change. Unlike the FDF, continuation analysis does not discard the higher harmonics of the heat release. It has already been applied to small thermoacoustic systems with $N \sim 10$ degrees of freedom [11–13]. With recent advances in matrix-free iterative methods, which require less computational time and less memory, it can now be applied to larger systems such as thermal convection [14]. Although a continuation analysis allows a rapid sweep over parameter values to explore behaviour, it does not provide a physical explanation of that behaviour. With the FDF at one's disposal, however, a physical understanding is provided via its description of the changes in the flame's gain and phase with varying forcing amplitude.

In this paper we combine the two methods to study the nonlinear dynamics of the Burke–Schumann flame under acoustic coupling. There are two advantages to this approach. First, their combination allows one to explore behaviour over a large parameter space using the continuation analysis, but also to explain that behaviour by using the FDF at interesting points in that parameter space. Second, since a continuation analysis makes use of the underlying model directly without discarding any of its dynamics, it can be used to validate the FDF. Specifically, since the main simplification made by the FDF is to discard higher harmonics of the flame's response, one can investigate how valid this simplification is.

Please cite this article in press as: S.J. Illingworth et al., *Proc. Combust. Inst.* (2012), http://dx.doi.org/10.1016/j.proci.2012.06.017

The paper is organized as follows. The unsteady Burke–Schumann flame and the acoustic model are described in Section 2. In Section 3 the matrix-free continuation methods are described, and continuation results over a range of parameters are presented. The FDF approach is employed in Section 4, and its prediction of the coupled system dynamics is compared to that given by the continuation methods of Section 3. An explanation of the near-linear dynamics seen at all forcing amplitudes is given in Section 5.

2. The unsteady Burke–Schumann flame

The Burke–Schumann flame is a simple model of a diffusion flame. It has been used to study the steady-state structure of non-premixed flames [15,16] and, more recently, their unsteady behaviour under acoustic coupling [6,8].

A schematic of the Burke–Schumann flame is given in Fig. 2. Fuel is delivered into the combustion zone in the middle slot of width $2\alpha H$, with co-flowing oxidizer delivered on either side. For thermoacoustic analysis, the flame sits in a simple open–open duct of length L at a distance x_f from the duct's upstream end. We assume a low Mach number mean flow in the duct. We assume one-step, infinite-rate chemistry; that the system is two-dimensional; that the density is constant; that the transverse velocity is zero; and that the axial velocity, although varying in time, does not vary in space. Combustion is assumed to be compact, which means that the flame is short in comparison with the acoustic wavelengths of interest.

2.1. The Z field and its boundary conditions

Choosing the mixture fraction, Z, as our passive scalar of interest, the transport equations for the two species reduce to a single non-dimensional equation:

$$\frac{\partial Z}{\partial t_c} + U\frac{\partial Z}{\partial x_c} = \frac{1}{\mathrm{Pe}}\left(\frac{\partial^2 Z}{\partial x_c^2} + \frac{\partial^2 Z}{\partial y_c^2}\right). \tag{1}$$

The combustion time- and length-scales, t_c, x_c, y_c are non-dimensionalized using the mean free-stream velocity and the flame half-width, H.

The boundary conditions are the same as those used in [7]. At the inlet we impose $Z = 1$ for the fuel slot ($|y_c| < \alpha$), and $Z = 0$ for the two oxidizer slots ($\alpha < |y_c| < 1$). Two more boundary conditions are imposed:

$$\frac{\partial Z}{\partial y} = 0 \quad \text{for } y_c = \pm 1,\ \forall\, x;$$

$$\frac{\partial Z}{\partial x} = 0 \quad \text{for } x_c \to \infty,\ \forall\, y_c;$$

which say that there is no flux of species at the wall; and that all quantities are bounded. (The second boundary condition is imposed at the downstream end of the flame's domain.)

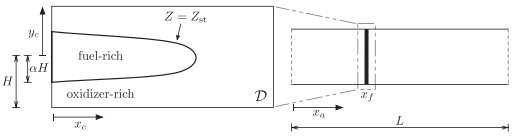

Fig. 2. The Burke–Schumann flame: (a) flame geometry and (b) duct geometry.

2.2. Temperature field

To find the heat release rate $Q(t)$, one must first relate the Z field to the temperature field, T [17]:

$$T(Z) = T_i + Z$$
oxidizer-rich region, $Z < Z_{st}$, (2a)

$$T(Z) = T_i + \frac{Z_{st}}{1 - Z_{st}}(1 - Z)$$
fuel-rich region, $Z \geqslant Z_{st}$. (2b)

Z_{st} is the stoichiometric mixture fraction and $Z = Z_{st}$ describes the flame surface (see Fig. 2). T_i is the inlet temperature.

2.3. Heat release rate

The total heat release rate, $Q(t) = \overline{Q} + q(t)$, is given by the rate of change of the temperature field, integrated over the whole domain. We must use the material derivative at each point in the domain $\mathscr{D}$ to account for the transport of fresh fuel and oxidizer into the domain:

$$Q(t) = \int_{\mathscr{D}} \left(\frac{\partial T}{\partial t} + U\frac{\partial T}{\partial x}\right) d\mathscr{D}. \tag{3}$$

The temperature field is discontinuous, so we must split this integral into the contributions from the fuel-rich region and from the oxidizer-rich region (see Fig. 2).

2.4. Numerical scheme

The Z field is solved using a Chebyshev discretization. Symmetry in y_c is assumed, and the solution is therefore on the half-domain only, $y_c \in [0, H]$. The grid has 31 Chebyshev points in the x_c-direction, and 17 points in the y_c-direction.

The top-hat boundary condition used at the inlet (i.e. $Z = 1$ for the fuel slot, $Z = 0$ outside it) is not well-suited to a Chebyshev discretization. However, the diffusive term in Eq. (1) ensures that this top-hat profile is smoothened some short distance from the inlet. An effective inlet is therefore defined a small distance from the top-hat profile. The mixture fraction profile at this location — which is provided by a separation-of-variables

Please cite this article in press as: S.J. Illingworth et al., *Proc. Combust. Inst.* (2012), http://dx.doi.org/10.1016/j.proci.2012.06.017

solution of the steady Z field — serves as the inlet boundary condition for the Chebyshev discretization.

2.5. Acoustics

For thermoacoustic analysis, acoustic perturbations are considered on top of the mean velocity. The perturbations are governed by the momentum and energy equations:

$$\frac{\partial u}{\partial t_a}+\frac{\partial p}{\partial x_a}=0;\quad \frac{\partial p}{\partial t_a}+\frac{\partial u}{\partial x_a}+\zeta p=\beta_T\delta_f q. \tag{4}$$

u and p are the non-dimensional perturbations in velocity and pressure. (The pressure has been non-dimensionalized using γM.) δ_f is the Dirac delta function; ζ represents acoustic damping; and $\beta_T=1/T_{\mathrm{ref}}$. Here T_{ref} is a non-dimensional reference temperature, $T_{\mathrm{ref}}=(T_i+T_{\mathrm{ad}})/2$, where T_{ad} is the adiabatic flame temperature, given by setting $Z=Z_{\mathrm{st}}$ in Eq. (2). The acoustic time- and length-scales, t_a, x_a are non-dimensionalized using the speed of sound and the duct length.

For the simple duct considered (see Fig. 2), $\partial u/\partial x$ and p are both set to zero at the ends of the tube. These boundary conditions are enforced by choosing basis sets that match them:

$$\begin{aligned} u(x_a,t_a)&=\sum_{j=1}^{N}\eta_j(t_a)\cos(j\pi x_a);\\ p(x_a,t_a)&=\sum_{j=1}^{N}\alpha_j(t_a)\sin(j\pi x_a). \end{aligned} \tag{5}$$

(For the momentum equation to be satisfied, $\eta_j(t_a)$ and $\alpha_j(t_a)$ must be related by $\alpha_j(t_a)=\dot\eta_j(t_a)/j\pi$.) The acoustic damping, ζ, is dealt with by assigning a damping parameter, ζ_j, to each mode:

$$\zeta_j=c_1 j^2+c_2 j^{1/2}. \tag{6}$$

This model is based on correlations developed by Matveev [18] from models in Landau and Lifschitz [19]. The Galerkin discretization of Eq. (5) leads to a state-space model relating the perturbation in heat release rate, $q(t)$, to the acoustic velocity perturbation at some point in the duct:

$$\dot\psi(t_a)=A\psi(t_a)+\beta_T B q(t_a), \tag{7a}$$

$$u(t_a)=C\psi(t_a), \tag{7b}$$

where ψ is the column vector $\psi=[\eta;\dot\eta]$ and A, B, C are suitably-dimensioned matrices. β_T remains a variable in Eq. (7a) to make clear that it enters linearly into the acoustics. β_T will serve as one of two parameters which will be varied in the continuation analysis of Section 3.

In Section 4 we will make use of the transfer function corresponding to Eq. (7). This is provided by taking Laplace transforms of Eq. (7) and substituting Eq. (7a) into Eq. (7b) to give $A(s)=C(sI-A)^{-1}B$, where s is the Laplace variable.

2.6. Combustion–acoustic coupling

The flame model (1) and the acoustic Eq. (4) use different non-dimensionalizations. Therefore one unit of combustion time, t_c, is not the same as one unit of acoustic time, t_a. An important parameter is their ratio, $t_c/t_a=ML/H$. (Recall that H is the half-width of the flame and L is the length of the duct.) ML/H is therefore important because varying it it controls the timescales of the flame dynamics with respect to the acoustic dynamics. (This was previously recognized in [6].) In this study we set $ML/H=1$, which means that combustion time and acoustic time are the same, $t_c=t_a$. This is sensible for a low Mach number ($M\ll 1$) and a compact flame ($L/H\gg 1$).

3. Matrix-free continuation of limit cycles

3.1. Method

This section describes the numerical method we use to find limit cycles. Ref. [20] contains a complete description. Continuation analysis examines nonlinear systems with evolution

$$\frac{\partial x(t)}{\partial t}=f(x(t),\lambda),\quad x(t)\in\mathbb{R}^N,\ \lambda\in\mathbb{R}, \tag{8}$$

where x is the system state with dimension N and λ are parameters. The state contains all the variables required to define the system. For the Burke–Schumann model, $x=[\eta,\dot\eta,Z]$, where η and $\dot\eta$ are the amplitudes of the acoustic modes and Z is the mixture fraction values on the Chebyshev grid.

Shooting methods are the most efficient way to find limit cycles of large systems. The shooting method used in this paper iterates to find a state on the limit cycle, $x(0)$, and the period of the limit cycle, T. The magnitude of the residual vector, $r=x(0)-x(T)$ (Fig. 3), is reduced to a predefined tolerance by a two-step iteration process. First, we consider the evolution of the system when started from small perturbations around our current guess $[x,T]$. We generate a $(N+1)\times(N+1)$ Jacobian matrix [21], which relates a general small change in $[x(0),T]$ to the resulting change in $[x(T),T]$. The spatial part of the Jacobian is defined as $\partial(x_i(0)-x_i(T))/\partial x_j(0)$. The jth column of the Jacobian matrix is formed by perturbing $x_j(0)$, then time-marching forward and seeing the resultant change in $x(T)$. To fill the matrix, we thus require N time-marches. Second, we solve a

Please cite this article in press as: S.J. Illingworth et al., *Proc. Combust. Inst.* (2012), http://dx.doi.org/10.1016/j.proci.2012.06.017

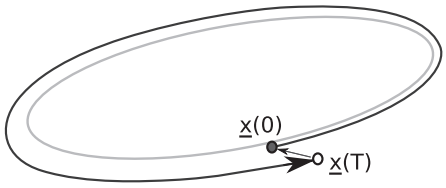

Fig. 3. Shooting method to find a limit cycle.

linear equation with the Jacobian matrix to find the $[\Delta x, \Delta T]$ that we should add to our current guess, $[x, T]$, in order to improve the guess. If the magnitude of the residual is still too large, we repeat the first step from the improved guess.

For large systems, it is impractical to form and store the Jacobian matrix. It is better to use matrix-free iterative methods, which inexactly solve the linear equations using only a few time-marches, without forming the Jacobian matrix. In this paper, we use the GMRES method [22]. Like many combustion, acoustic, and fluid mechanical systems, our thermoacoustic system is dissipative, which means that only a few bulk fluid motions are influential in the long time limit. Consequently, in each limit cycle, there are far fewer influential degrees of freedom than there are variables. GMRES inexactly solves the linear equations by implicitly using these influential bulk motions, while ignoring features that are quickly dissipated. Importantly, although the $[\Delta x, \Delta T]$ steps are calculated by an inexact method which uses only the influential bulk motions of the system, the limit cycle found by the iterative process uses the full system and is therefore exact. The stability of a converged limit cycle is defined by its Floquet multipliers, which are the eigenvalues of the matrix $\partial x_j(T)/\partial x_j(0)$. The eigenvalues are calculated using the matrix-free Krylov–Schur algorithm [20].

3.2. Results

Figure 4 shows the limit cycle amplitudes as two parameters are varied: Peclet number, which changes the ratio of advection to diffusion in the flame, and β_T, which controls the extent to which unsteady combustion perturbs the acoustics (Eq. (7a)). The parameters that are held fixed are $Z_{st} = 0.8$, $c_1 = 0.0247$, $c_2 = 0.018$, $\alpha = 0.35$, $x_f = 0.25$, $ML/H = 1$. There are 20 acoustic modes and Z is solved on a 31×17 Chebyshev grid. Each limit cycle is calculated to a tolerance of $\|x(0) - x(T)\| < 10^{-8}$.

The Hopf bifurcation marks the boundary between linearly stable and linearly unstable operating conditions. The limit cycles form a surface which has both subcritical bifurcations for $50 < \mathrm{Pe} < 70$ (Fig. 4(a)) and supercritical bifurcations for $\mathrm{Pe} < 50$, $\mathrm{Pe} > 70$ (Fig. 4(c)). Where there is a subcritical bifurcation, there is a stable limit cycle at higher velocity amplitudes. However, this stable limit cycle has velocity amplitudes >2 and is not shown in the figure. The bistable operating conditions are those at which the system is linearly stable but can be triggered to a high amplitude limit cycle.

The limit cycles describe the behaviour of the fully coupled system, and are calculated by continuation analysis quite cheaply: the Hopf bifurcation line takes roughly 500 s and the surface of limit cycles takes 61 CPU hours. The surface is composed of 70 slices and roughly 2500 converged limit cycles, requiring an average of 52 minutes per slice, and 90 seconds per limit cycle. The computation can be easily parallelized because the surface is composed of separate two-dimensional slices.

The relative computational expense of the FDF and of a continuation analysis depends on the stability information that is required. If the flame operating condition is fixed and the acoustic operating condition is varied, then only one FDF evaluation is required, and the FDF does not fare too badly in a comparison (in this case 52 CPU minutes for one slice of the continuation surface, versus 17 CPU hours for one FDF evaluation). If both the flame and the acoustic operating conditions are varied, however, then the FDF must be re-evaluated at each of the flame's operating conditions, and this is expensive. The major advantage of the continuation method over the FDF is that its computational cost does not depend on the type of system parameter that one varies. This means that it can calculate the stability limits when both the flame and the acoustic operating conditions are varied, and does so with a modest expense. Returning to Fig. 4, the Peclet number determines the flame operating condition, while T_{ref} determines the acoustic operating condition. This means that a separate FDF evaluation is required for each constant-Peclet number slice. One FDF evaluation requires approximately 17 CPU hours, so the FDF would require approximately 1120 CPU hours to produce Fig. 4. This is more than an order of magnitude greater than that required by continuation.

4. A flame describing function approach

In this section we investigate the Burke–Schumann flame's nonlinear dynamics using the flame describing function (FDF) technique. In a linear setting, one can characterize a flame's response to forcing by measuring its gain and phase over a range of forcing frequencies (its transfer function). Such a characterization is useful but it cannot predict the flame's — and therefore the coupled system's — nonlinear dynamics, such as limit cycle amplitudes and frequencies.

Please cite this article in press as: S.J. Illingworth et al., *Proc. Combust. Inst.* (2012), http://dx.doi.org/10.1016/j.proci.2012.06.017

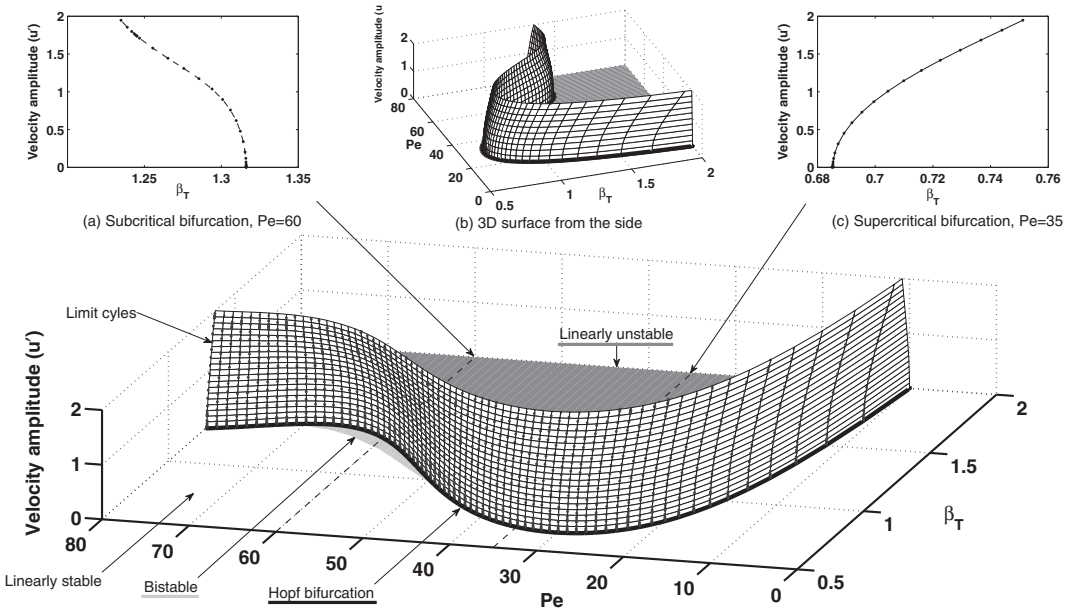

Fig. 4. Continuation results for limit cycle amplitudes. The thick dark line is the Hopf bifurcation, which is the same as the linear stability limit. The linearly unstable region is shaded dark gray and the bistable region is shaded light gray (the bistable region is the vertical shadow of the subcritical bifurcation). Limit cycles are shown as dark dots on a surface interpolated between neighbouring slices. The surface exhibits both subcritical bifurcations (a) and supercritical bifurcations (c), where stable limit cycles are shown with a solid line and unstable limit cycles with a dashed line. The bifurcation diagrams at Pe = 60 and Pe = 35 will be compared with predictions given by the FDF in Section 4.

One way to address this is to use a describing function approach. In this setting, the flame's response to harmonic forcing is characterized over different forcing frequencies and, crucially, over different forcing amplitudes. The key assumption is that for a given forcing frequency, the flame responds predominantly at that frequency, and any higher harmonics in the flame's response are neglected.

The describing function was first employed by Dowling in her numerical studies [4,9], using which limit cycle amplitudes were well-predicted. The approach was then employed experimentally by Noiray et al. [10], who measured the describing function for a burner with multiple anchored flames, and who successfully predicted both supercritical and subcritical bifurcations using a dispersion relation for the acoustics. Durox et al. [23] obtained the FDF for four different flame geometries: a single conical flame; a V flame; an M flame, and a collection of conical flames, while Palies et al. [24] obtained the FDF of a premixed swirling flame. More recently, Boudy et al. [25] have used an FDF approach to investigate nonlinear triggering and mode switching.

4.1. The Burke–Schumann model's FDF

The Burke–Schumann model's FDF has been determined by forcing it harmonically at frequencies between 0.025 and 2.000, in increments of 0.025, and at forcing amplitudes between 0.1 and 1.0, in increments of 0.1. We denote the resulting flame describing function $F(i\omega, |u|)$, whose gain and phase is plotted in Fig. 5 for Peclet numbers of 35 and 60. These Peclet numbers correspond to the subcritical and supercritical slices in Fig. 4. For clarity, only data for the smallest forcing amplitude, $F(i\omega, 0.1)$, and the largest forcing amplitude, $F(i\omega, 1.0)$ are shown.

Let us first consider the FDF at the lowest forcing amplitude, $F(i\omega, 0.1)$, which we may assume represents the flame's linear frequency response.[1] The gain and phase plots for both Peclet numbers are similar to a first-order lag-type system, whose frequency response is given by $a/(i\omega + a)$ for some constant a. The gain is unity (0 dB) at low frequencies and decreases with increasing frequency. The phase is 0° at zero frequency, and approaches approximately −60° at high frequencies. (This differs from the −90° phase change seen at high frequencies for a pure first-order lag system.)

[1] This has been verified by computing the FDF for a forcing amplitude of 0.01. The differences in gain and in phase are always less than 0.06%, which is true for both Peclet numbers. Therefore the 0.1 amplitude data can be treated as the linear forcing limit.

Please cite this article in press as: S.J. Illingworth et al., *Proc. Combust. Inst.* (2012), http://dx.doi.org/10.1016/j.proci.2012.06.017

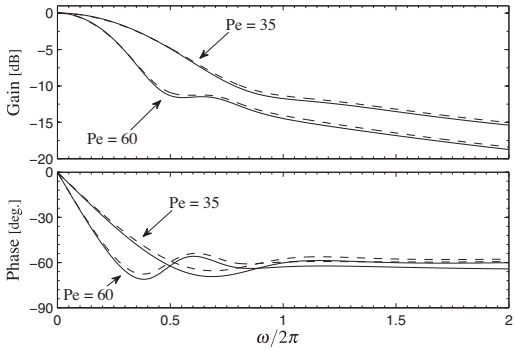

Fig. 5. Flame describing function normalized by the mean heat release, $F(i\omega,|u|)/Q$ for Peclet numbers of 35 and 60. The response for the smallest forcing, $F(i\omega,0.1)$ (---) and the largest forcing, $F(i\omega,1.0)$ (——) are shown.

Let us now consider the largest forcing amplitude case, $F(i\omega,1.0)$. Perhaps surprisingly, the changes in gain and phase across the two forcing amplitudes are very small. At $\mathrm{Pe}=35$, for example, the maximum changes in gain and phase across all frequencies are 0.014 and 4.9°. Although the current study is for a diffusion flame, this behaviour is consistent with previous studies on premixed flames, where it has been observed that a spatially constant velocity field is an overly crude approximation [26], and that it can give rise to flame dynamics that are nearly linear with respect to forcing amplitude [27]. It is likely that a convective velocity model would give rise to richer nonlinear behaviour.

A second characterization of the flame's nonlinear behaviour is provided by the amplitude of its higher harmonics. Defining a gain for the second harmonic, for example, gives the flame's gain at frequency 2ω when it is forced harmonically with frequency ω. This is done in Table 1, which shows the maximum gains across all frequencies for the second, third and fourth harmonics. Data for the largest forcing amplitude of 1.0 have been used, since this is where we expect higher harmonics to be largest. The largest gain is seen in the second harmonic, but even this is only around 5% of the FDF's maximum gain (which is unity, Fig. 5). The gain is smaller still in the third and fourth harmonics.

These small changes in dynamics with increasing forcing amplitude help to explain the very large limit cycles seen in Fig. 4. For a linearly unstable system, a (stable) limit cycle will be reached when the system's nonlinear dynamics are sufficiently different from the linear dynamics to permit the limit cycle. Since linear acoustics are assumed, the FDFs of Fig. 5 imply that if the coupled system is linearly unstable, it will remain unstable even for large-amplitude oscillations.[2] The same argument holds when the coupled system is linearly stable. We now consider this point in more detail, drawing on the FDF and Nyquist's stability criterion to predict and explain the behaviour seen at Peclet numbers of 35 and 60.

Table 1
Maximum gain across all frequencies for the flame's second, third and fourth harmonics.

Pe	2nd harm.	3rd harm.	4th harm.
35.0	0.0528	0.0225	0.0083
60.0	0.0322	0.0179	0.0093

4.2. Predicting behaviour with the FDF

We now consider how the FDF can be used to predict the bifurcation behaviour of the coupled thermoacoustic system. To do so, one must model the interaction of the nonlinear flame with the linear acoustics of Section 2.5. Noiray et al. [10] achieve this by developing a dispersion relation which, upon feeding in the FDF and solving, provides growth rates and eigenfrequencies over a range of forcing amplitudes.

A different approach is taken in this paper. Following Dowling [4,9], in the present quasi-linear setting, the eigenfrequencies of the coupled system are those points in the complex s-plane satisfying

$$1+F(s,|u|)A(s)=0. \tag{9}$$

(We have replaced $i\omega$ with the Laplace variable s here to allow complex frequencies, but we will shortly revert back to $s=i\omega$.) $A(s)$ is the acoustic transfer function (see Section 2.5).

It is convenient to investigate the roots of Eq. (9) by using its Nyquist curve. This involves plotting $F(s,|u|)A(s)$ in the complex plane for real frequencies, $s=i\omega$. Nyquist's stability criterion says that if the Nyquist curve of $F(i\omega,|u|)A(i\omega)$ encircles the -1 point (the 'critical point'), then the

[2] Higher acoustic damping will give rise, in principle, to smaller limit cycles. However, higher damping also means that linear instability is less likely in the first place. That is, damping must be smaller than driving for the system to be linearly unstable, and they must become equal in the limit cycle. The only way this can happen (i.e. for their relative sizes to change) is via the nonlinear dynamics of the flame, since the acoustics are linear. Therefore since the changes in the flame's dynamics with forcing amplitude are so small, a reasonably-sized positive growth rate gives rise to very large limit cycles, and the only way a small limit cycle can exist is when the growth rate in the linear limit is only just positive.

Please cite this article in press as: S.J. Illingworth et al., *Proc. Combust. Inst.* (2012), http://dx.doi.org/10.1016/j.proci.2012.06.017

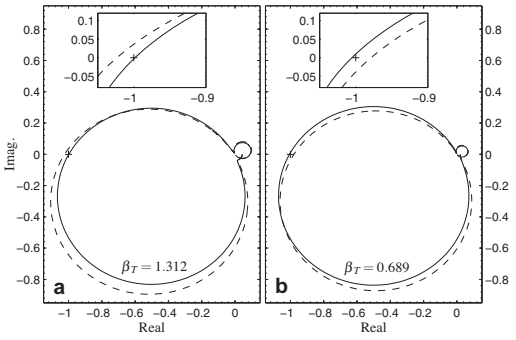

Fig. 6. Nyquist curves (positive frequencies only) for the (a) subcritical (Pe = 60) and (b) supercritical (Pe = 35) cases. The locus of $F(i\omega,|u|)A(i\omega)$ is shown for the smallest (—) and largest (– –) forcing amplitudes. The inset zooms in around the −1 point.

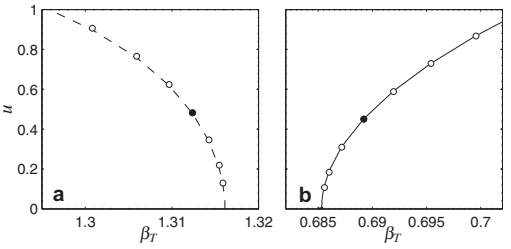

Fig. 7. The Nyquist curves' predictions (○) of (a) the subcritical (Pe = 60); and (b) the supercritical (Pe = 35) bifurcations over a range of β_T. The β_T used in Fig. 6 are marked with (•). The solid and dashed lines represent the limit cycle amplitudes given by the continuation analysis in Fig. 4.

coupled system will be unstable (i.e. positive growth rate). If the Nyquist curve of $F(i\omega,|u|)A(i\omega)$ does not encircle the −1 point, then the coupled system will be stable (i.e. negative growth rate).

The implications for our quasi-linear analysis using the FDF are immediate. Since encirclement of the −1 point corresponds to a positive growth rate, and a lack of an encirclement corresponds to a negative growth rate, a growth rate of zero must result when the Nyquist curve of $F(i\omega,|u|)A(i\omega)$ passes exactly through the −1 point.

This is demonstrated in Fig. 6. Let us first consider Fig. 6(b), which represents the supercritical bifurcation at Pe = 35. (The two plots are this way round to be consistent with Fig. 4.) The Nyquist curves of $F(i\omega,|u|)A(i\omega)$ are shown (for positive frequencies only) for the smallest and largest forcing amplitudes. The inset zooms in around the −1 point. We see an encirclement of the −1 point for the smaller forcing amplitude of 0.1. At a forcing amplitude of 1.0, however, this encirclement has been lost. We therefore expect a linearly unstable system for small forcing amplitudes, and a stable limit cycle which has an amplitude of less than one.

Figure 6(a) performs the same analysis for the subcritical slice (Pe = 60) of Fig. 4. In this case we expect the FDF to reveal a linearly stable flame which, for larger forcing amplitudes, becomes nonlinearly unstable, and this is what we see in Fig. 6(a). There are no encirclements of the critical point for the smallest forcing amplitude, but the critical point is encircled for the largest forcing amplitude.

At this point, the FDF has predicted the supercritical bifurcation at Pe = 35 and the subcritical bifurcation at Pe = 60, but it has not predicted the amplitudes of the limit cycles. To find the limit cycle amplitudes we must do two things. First, for each forcing amplitude, find the point where the Nyquist curve passes through the negative real axis. Second, interpolate these values to find the amplitude at which the Nyquist curve passes exactly through the −1 point. The results of this procedure are shown in Fig. 7, where the FDF's prediction of the limit cycle amplitude is compared to that given by the continuation analysis. Since the parameter β_T only affects the acoustics and does not affect the flame dynamics directly, we can do this for a range of β_T. (The comparison is made only for limit cycle amplitudes between 0.1 and 1.0, since this is the range of amplitudes over which FDF data are available.) We see excellent agreement between the FDF results and the continuation analysis. In addition, the same analysis has been performed at Peclet numbers of 10 and 80, for which the FDF performs equally well in predicting the limit cycle amplitudes. This suggests that the approximations made in forming the FDF — namely, that higher harmonics of the flame's response may be neglected — are valid for the Burke–Schumann model under investigation. An important question is whether the supercritical and subcritical bifurcations are caused by changes in gain or in phase of the Burke–Schumann flame's response. Figures 5 and 6 tell us that it is a combination of the two. In Fig. 5 we see that, for both Peclet numbers, there are changes both in gain and in phase with forcing amplitude. Relating this to the Nyquist curve in Fig. 6, a change in gain will act to expand or shrink the entire Nyquist curve, while a change in phase will rotate it. Both of these effects influence whether the critical point is encircled or not, and so both affect the coupled thermoacoustic system's bifurcation behaviour.

It would be interesting to also look at the effect of the flame position and the mode-dependent acoustic damping on the FDF's level of success. These two parameters would impact the validity of the FDF by changing the relative sizes of the different acoustic modes. It is likely that the

Please cite this article in press as: S.J. Illingworth et al., *Proc. Combust. Inst.* (2012), http://dx.doi.org/10.1016/j.proci.2012.06.017

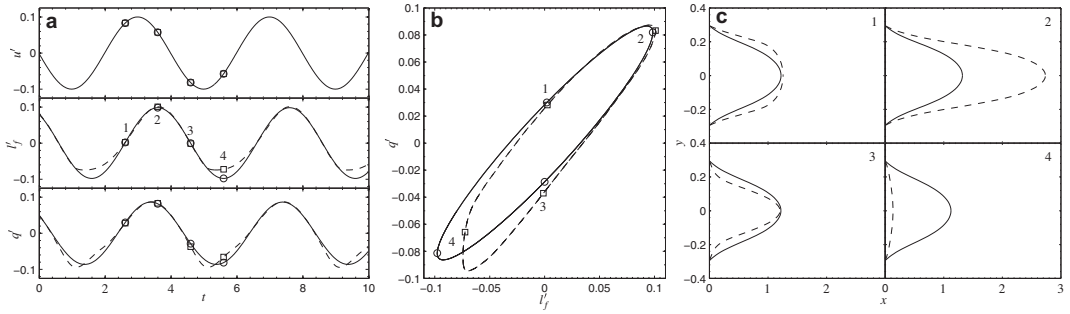

Fig. 8. Harmonic forcing of the flame at a frequency of 0.25: (a) forcing velocity u and the resulting perturbations in the flame length, l_f and heat release rate, q for forcing amplitudes of 0.1 (—) and 1.5 (––); (b) corresponding phase portrait; and (c) snapshots of flame shape at times indicated in parts (a, b). In (a, b), data for the largest forcing amplitude are scaled by 0.1/1.5 to allow a direct comparison.

FDF would still work well as these are varied for the current Burke–Schumann model, since the nonlinear harmonics generated by the flame are so small, but this would nonetheless be an interesting area for future work.

5. An explanation of the flame's dynamics

The results of Sections 3 and 4 suggest that the Burke–Schumann flame exhibits a near-linear response for all forcing amplitudes. In this section an explanation of this near-linear behaviour is given in the time domain at a Peclet number of 35.

Figure 8(a) shows the flame's response to a harmonic forcing frequency of 0.25 for forcing amplitudes of 0.1 and 1.5. (In the absence of acoustic coupling.) A scaling factor of 0.1/1.5 is applied to the larger forcing amplitude data to allow a direct comparison in the same plot. The forcing velocity, u, the perturbation in the flame length from steady-state, denoted l_f, and the perturbation in the heat release rate, q are plotted. The response at the two forcing amplitudes is remarkably similar for most of the cycle. The largest differences occur when the flame is shortest.

The phase portrait for q and l_f is given in Fig. 8(b). For the smallest forcing amplitude, a narrow ellipse is traced out, which suggests a small phase difference between q and l_f. For the largest forcing amplitude, this ellipse is distorted, but only during the part of the cycle where the flame is shortest and therefore closest to the inlet.

Figure 8(c) shows snapshots of the two flame shapes at the instances indicated in Fig. 8(a) and (b) (without any scaling). The second and fourth snapshots are the most important. The second snapshot shows the two flames at their longest. At this instant the two flames are self-similar since their scaled lengths and scaled heat release perturbations are almost identical (Fig. 8(a)). The fourth snapshot shows the two flames at their shortest and shows that the flame moves very close to the inlet for the higher forcing amplitude. Even though the maximum velocity perturbation ($u = 1.5$) is larger than the mean velocity (which is unity), the flame cannot traverse the inlet because of the boundary condition imposed there (see Section 2.1). It is around this part of the cycle that the two flames' behaviours differ most significantly (Fig. 8(a)).

Let us summarize this behaviour in two parts. First, the perturbation in the flame length varies almost linearly with the velocity amplitude: as the forcing amplitude increases, the flame length simply deviates proportionally from its steady-state value. If the forcing amplitude is sufficient to bring the flame tip close to the inlet, however, then the inlet boundary condition brings the flame to a halt, and the deviation in the flame length saturates during the negative part of the cycle. Second, there is a near-linear relationship between the flame length and the heat release, which persists at all forcing amplitudes, most clearly seen in Fig. 8(b). This breaks down if the flame tip approaches the inlet, and this appears to be the main source of nonlinearity in the current Burke–Schumann model.

It is clear that some aspects of the flame model are too simple to capture nonlinear behaviour at sensible forcing amplitudes. The flame responds nearly linearly nearly all of the time, and any nonlinearity is seen when the flame is close to the inlet. To address this, future work will look at the impact of two mechanisms which the current model does not include: a finite chemistry rate; and a spatially-varying velocity field.

6. Conclusions

The nonlinear thermoacoustic behaviour of a diffusion flame has been considered using two different approaches. The first, a continuation analysis, allows limit cycle amplitudes and frequencies to be rapidly found over a large parameter space, and no approximations of the underlying model

Please cite this article in press as: S.J. Illingworth et al., *Proc. Combust. Inst.* (2012), http://dx.doi.org/10.1016/j.proci.2012.06.017

are needed to use it. A physical interpretation of the results is not possible with this approach, however. The second approach involves finding the flame's response to harmonic forcing over a range of forcing frequencies and forcing amplitudes to generate a flame describing function (FDF). This is more time-consuming and is only valid for one set of flame parameters, but a physical interpretation of the results follows quite naturally.

By combining these approaches, two matters have been addressed. First, the FDF has been validated by comparing its prediction of limit cycle amplitudes to those given by the continuation analysis. The agreement is excellent. The FDF discards higher harmonics of the flame response, retaining only its response at the forcing frequency. Therefore the FDF's success suggests that, for this configuration, changes in gain and phase at the frequency of forcing dominates the Burke–Schumann flame's (mildly) nonlinear behaviour. Second, combining the two techniques allows one to rapidly sweep over many operating conditions using the continuation analysis; and to explain that behaviour at points of interest using the FDF.

The flame's response to forcing is nearly linear even for very large forcing amplitudes. An investigation in the time domain reveals that the (mild) nonlinearity in the flame response is mainly caused by the inlet boundary condition during the part of the cycle where the heat release rate (and flame length) is near its minimum. It seems that the current model is too simple to capture any other nonlinear dynamics of the flame. Future work will address this by considering the effects of a spatially-varying velocity field, which is known to be important in premixed flames [26], and which is likely to give rise to richer nonlinear dynamics in the Burke–Schumann flame. This will allow the application of the techniques presented in this paper to a flame model with a more realistic nonlinear response.

References

[1] A.P. Dowling, J.E. Ffowcs Williams, *Sound and Sources of Sound*, Ellis Horwood, 1983.
[2] G.A. Richards, M.C. Janus, *J. Eng. Gas Turbines Power* 120 (2) (1998) 294–302.
[3] T. Lieuwen, Y. Neumeier, B.T. Zinn, *Combust. Sci. Technol.* 135 (1998) 193–211.
[4] A.P. Dowling, *J. Fluid Mech.* 346 (1997) 271–290.
[5] M. Tyagi, N. Jamadar, S.R. Chakravarthy, *Combust. Flame* 149 (2007) 271–285.
[6] M. Tyagi, S.R. Chakravarthy, R.I. Sujith, *Combust. Theory Model.* 11 (2) (2007) 205–226.
[7] K. Balasubramanian, R.I. Sujith, *J. Fluid Mech.* 594 (2008) 29–57.
[8] K. Balasubramanian, R.I. Sujith, *Combust. Sci. Technol.* 180 (2008) 418–436.
[9] A.P. Dowling, *J. Fluid Mech.* 394 (1999) 51–72.
[10] N. Noiray, D. Durox, T. Schuller, S. Candel, *J. Fluid Mech.* 615 (1) (2008) 139–167.
[11] C.C. Jahnke, F.E.C. Culick, *J. Propul. Power* 10 (4) (1994) 508–517.
[12] M.P. Juniper, *J. Fluid Mech.* 667 (2011) 272–308.
[13] P. Subramanian, S. Mariappan, R.I. Sujith, P. Wahi, *Int. J. Spray Combust. Dynam.* 2 (4) (2010) 325–355.
[14] J. Sánchez, M. Net, B. Garcia-Archilla, C. Simó, *J. Comput. Phys.* 201 (1) (2004) 13–33.
[15] S.P. Burke, T.E. Schumann, *Indust. Eng. Chem.* 29 (1928) 998.
[16] J. Barr, *Proc. Combust. Inst.* 4 (1) (1953) 765–771.
[17] T. Poinsot, D. Veynante, *Theoretical and Numerical Combustion*, RT Edwards, Inc., 2005.
[18] K. Matveev, *Thermoacoustic Instabilities in the Rijke Tube: Experiments and Modeling*, Ph.D. thesis, California Institute of Technology, 2003.
[19] L.D. Landau, E.M. Lifshitz, *Fluid Mechanics*, Pergamon Press, 1959.
[20] I.C. Waugh, S.J. Illingworth, M.P. Juniper, *J. Comput. Phys.*, submitted for publication.
[21] D. Roose, K. Lust, A. Champneys, A. Spence, *Chaos Solit. Fract.* 5 (10) (1995) 1913–1925.
[22] Y. Saad, M.H. Schultz, *SIAM J. Sci. Stat. Comput.* 7 (3) (1986) 856–869.
[23] D. Durox, T. Schuller, N. Noiray, S. Candel, *Proc. Combust. Inst.* 32 (1) (2009) 1391–1398.
[24] P. Palies, D. Durox, T. Schuller, P. Morenton, S. Candel, *Comptes Rendus Mécanique* 337 (2009) 395–405.
[25] F. Boudy, D. Durox, T. Schuller, S. Candel, *Proc. Combust. Inst.* 33 (1) (2011) 1121–1128.
[26] T. Schuller, S. Ducruix, D. Durox, S. Candel, *Proc. Combust. Inst.* 29 (1) (2002) 107–113.
[27] T. Lieuwen, *Proc. Combust. Inst.* 30 (2) (2005) 1725–1732.

Please cite this article in press as: S.J. Illingworth et al., *Proc. Combust. Inst.* (2012), http://dx.doi.org/10.1016/j.proci.2012.06.017